RSC Advances

ROYAL SOCIETY OF CHEMISTRY

www.rsc.org/advances

Polyethylenimine mediated magnetic nanoparticles for combined intracellular imaging, siRNA delivery and anti-tumor therapy

Xueqin Wang*, Liang Zhu, Xuandi Hou, Liang Wang, Shijiao yin

College of Bioengineering, Henan University of Technology, Zhengzhou, Henan 450001, P.R .China

** Corresponding author: Xueqin Wang, College of Bioengineering, Henan University of Technology, Zhengzhou, Henan 450001, P.R .China. Tel.: + 86 371 67756928; fax: + 86 371 67756928. E-mail address:* wangxq0708@163.com (X.Wang).

Abstract

Magnetic nanocarrier assisted delivery of small interfering RNA (siRNA) represents a promising approach for tumor treatment by efficiently down-regulating expression of key tumorigenic genes, which has been proven feasible and effective for anti-tumor therapy. In the present study, the polyethylenimine (PEI) mediated magnetic nanoparticles (PEI-MNPs) were synthesized as carriers for tumor treatment by combined bioimaging, siRNA delivery and in vitro therapy of glioblastoma multiforme, and their direct biological activity was elucidated in the treated tumor cells. The results demonstrated that the synthesized PEI-MNPs not only had a very low cytotoxicity in the studied concentrations, but they also showed the loading of siRNA molecules could form stable siRNA loaded PEI-MNPs complex (siRNA~PEI-MNPs) in the tested serum. In addition, the intracellular imaging showed that the PEI-MNPs could efficiently enter the tumor cells and approach the nuclei after being uptaken, which were monitored through fluorescent magnetic labeling. The fabricated siRNA~PEI-MNPs

displayed a very much better therapeutic efficiency to inhibit cell proliferation, and induce cell apoptosis and autophagy of glioblastoma U251 cells, which was confirmed by analysis of biological activity in the treated cells. Therefore, this study suggested that the fabricated PEI-MNPs were a promising non-viral nanovehicle for the combined intracellular imaging and siRNA delivery for an efficient anti-tumor therapy based on siRNA therapeutic strategy, and the siRNA~PEI-MNPs could be of great use for anti-tumor treatment in glioblastoma multiforme in future.

Keywords: Magnetic nanoparticles, Polyethylenimine, Small interfering RNA, Intracellular imaging, Glioblastoma multiforme

1 Introduction

Glioma, especially glioblastoma multiforme (GBM, World Health Organization/ WHO grade IV), is the most common and aggressive type of malignant brain tumor, accounting for about half of all the primary brain tumors. GBM can arise either *de novo* or as a result of malignant progression of a low-grade glioma.[1] Malignant glioma has a poor prognosis and remains virtually incurable despite aggressive treatment by surgery, radiotherapy and chemotherapy.[2, 3] The highest incidence is in the older population and the 2-year survival rate is less than 3% .[4] The median survival is only 12-15 months for patients with glioblastomas and 2-5 years for patients with anaplastic gliomas.[5] Therefore, tremendous efforts have been made to develop effective therapeutic strategies for anti-tumor therapy in glioma treatments. Survivin, a new member of the inhibitors of apoptosis (IAP) family, has functional role in both cell division

and apoptosis control [6, 7], and is often found to be up-regulated in tumors, enabling it a potential new target for tumor treatment. Currently, down-regulating the expression of survivin gene by siRNA becomes an effective therapeutic modality for tumors.[8-11]

Small interfering RNA (siRNA), consisting of double-stranded RNA molecules of 20-25 nucleotides, catalyzes target mRNA cleavage by forming an RNA-induced silencing complex (RISC) and interferes with the expression of specific proteins encoded by mRNA, which provides a promising therapeutic method for serious diseases, especially various tumors because of their superior ability to down-regulate the expression of target genes in a specific manner.[12-14] However, the use of naked siRNA in clinical applications has been restricted by its very poor intracellular uptake, failure of endosomal escape, rapid enzymatic degradation in the bloodstream, low delivery efficiency to target cells, and nonspecific gene suppression (off-target effects).[15] Thus, clinical use of siRNA needs adequate delivery strategies to both protect the RNA from enzymatic degradation and to reach the action site in the targeted cells.

Many siRNA-carrier systems, including viral and nonviral systems have been widely exploited to surmount these limitations and to enhance intracellular uptake and stability against nucleases.[16-18] Although transfection is highly efficient, viral vectors, including adenovirus, adeno-associated virus, and retrovirus, are strictly limited due to its immunogenicity, potential pathogenicity, endogenous recombination and laborious preparation.[19, 20] In contrast, non-viral vectors have drawn high attention because of their potential advantages including no risk of infection, low toxicity, good biocompatibility, non-pathogenicity and non-immunogenicity, and can be prepared and modified relatively easily.[21, 22] However, low transfection efficiency has limited their use in therapeutic

applications compared with viral systems. Hence, the lack of appropriate vector has become a major hurdle in the development of siRNA therapy for severe diseases including tumors.[23-25] The development of appropriate carrier systems is crucial for practical applications of siRNAs as therapeutics. Currently several nanoparticle as non-viral siRNA delivery systems, such as gold nanoparticles, various polymer nanoparticles, quantum dots (QD) and/or functional molecules modified QD, have been developed to overcome the major hurdles facing the therapeutic siRNA delivery due to their biocompatibility and biodegradability, efficient translocation, size diversity, easily surface functionalization and immobilization with various moieties [26,27]. However, there are critical issues such as immune responses, cytotoxicity, and off-target [26,27]. Magnetic nanoparticles, particularly magnetite (Fe_3O_4) and/or maghemite (γ-Fe_2O_3), are highly feasible carriers for siRNA delivery owing to their unique properties such as uniform size, nontoxicity, large surface area, biocompatibility, superior stability in body fluids, nonimmunogenicity, and facile surface modification for cell-specific targeting and imaging/tracking. Moreover, cationic liposome, polyethylenimine (PEI), poly (L-lysine), and their various derivatives are frequently exploited as nonviral delivery systems.[28-30] Especially, Polyethylenimine (PEI) is currently the most popular cationic polymer used in non-viral gene delivery due to its high transfection efficiency and superior ability to escape from endosomes via a “proton-sponge” effect.[31-33] Accordingly, various types of PEI-based cationic copolymers have been developed to improve the delivery efficiency and gene silencing effect of siRNA.[34, 35] Therefore, the development of PEI-modified magnetic nanoparticles (PEI-MNPs) is a superior strategy for siRNA delivery and efficient transfection in the practical applications of siRNA-induced target gene silencing in the effective

therapeutic of tumors.

In the present study, the positively charged PEI was grafted with MNPs to synthesize PEI-modified MNPs (PEI-MNPs), and the size and shape, the structure composition, cytotoxicity and intracellular uptake of the PEI-MNPs were then characterized. The PEI-MNPs were subsequently intracellular imaging, and utilized as carries to load survivin-targeted siRNA molecules designed for potentially silencing endogenous survivin expression in glioblastoma multiforme U251 cells, and their direct biological activity was investigated in detail.

2 Experimental section

2.1 Reagents and materials

Superparamagnetic γ-Fe_2O_3 nanoparticles (MNPs) utilized in this study were prepared from magnetite (Fe_3O_4) according to methods proposed elsewhere.[36, 37] The human glioblastoma U251 cell line was obtained from the Shanghai Cell Bank of the Chinese Academy of Sciences (Shanghai, China). The cell culture medium and the fetal bovine serum (FBS) were purchased from Gibco Invitrogen Corporation (CA, USA). Polyethylenimine (PEI), 3-(4,5-dimethylthiazol-2-diphenyl-tetrazolium) bromide (MTT), fluorescein isothiocyanate (FITC), fluorescein diacetate (FDA), propidium iodide (PI), Hoechst H33258, acridine orange (AO), dimethyl sulfoxide (DMSO), Triton X-100 solution, and paraformaldehyde were purchased from Sigma-Aldrich (St. Louis, MO, USA). Monoclonal mouse anti-LC3 A/B antibody and Alexa Fluor 488 goat anti-mouse IgG were obtained from Proteintech Group, Inc. (Chicago, IL, USA). Fluorescent dye 4, 6-diamidino-2-phenylindole (DAPI) was purchased from Molecular Probes Inc. (Eugene,

OR, USA). Rhodamine phalloidin was obtained from Cytoskeleton Inc. (Denver, CO, USA). TRIzol reagent was acquired from Invitrogen (Carlsbad, CA, USA). M-MLV reverse transcriptase were purchased from Promega (Madison, WI, USA). SYBRH Premix Ex Taq^{TM} were purchased from Takara (Kyoto, Japan). Other reagents and chemicals were purchased from local commercial suppliers and were of analytical reagent grade, unless otherwise stated. Deionized (DI) water (Milli-Q, Millipore, Bedford, MA) was used to prepare aqueous solutions. The duplexed unlabeled survivin siRNA, 5'-carboxyfluorescein (FAM) labeled and scrambled survivin siRNA were synthesized with the following sequences by Shanghai GenePharma Co., Ltd (sense, 5'-CACCGCA UCUCUACAUUCATT-3';antisense, 5'-UGAAUGUAGAGAUGCGGUGTT-3'; Negative control, sense, 5'-UUCUCCGAACGUGUCACGUTT-3'; antisense, 5'-ACG UGACACGUUCGGAGAATT-3').

2.2 Principle for PEI-MNPs mediated intracellular imaging and siRNA delivery for gene silencing

The general principle of the PEI-MNPs mediated intracellular imaging, siRNA delivery and anti-tumor therapy for human malignant glioblastoma multiforme U251 cells (Figure 1) starts with the preparation of PEI-MNPs by combining magnetic γ-Fe_2O_3 nanoparticles (MNPs) and PEI, which were then modified by using FITC. Subsequently, the FITC labeled PEI-MNPs (FITC-PEI-MNPs) were internalized into glioblastoma multiforme U251 cells for intracellular imaging. Simultaneously, the PEI-MNPs were also loaded with survivin siRNA through electrostatic attraction, which was finally delivered into the glioblastoma cells. The intracellular uptake, siRNA delivery efficiency and anti-tumor effects were investigated

against glioblastoma multiforme U251 cells.

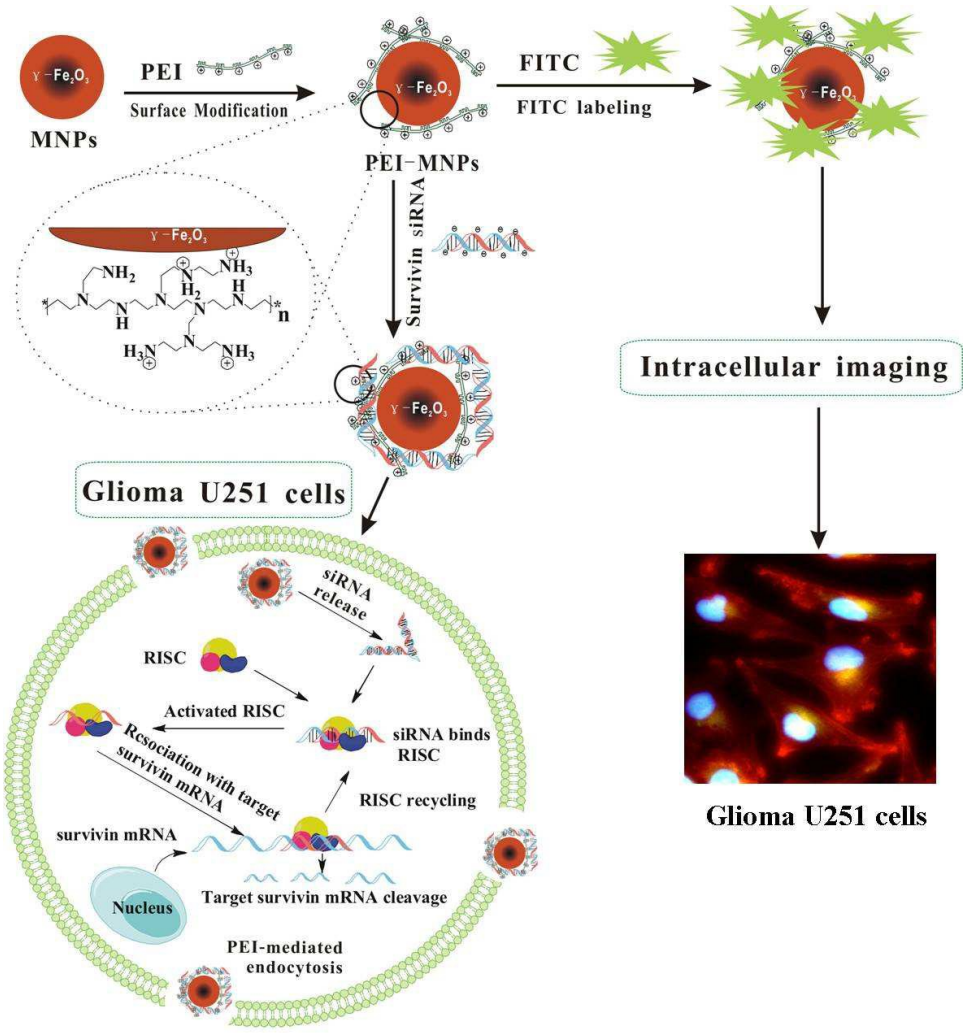

Figure 1 Schematic representation of the PEI-MNPs mediated intracellular imaging, and as carriers for survivin siRNA delivery in tumor U251 cells.

2.3 Synthesis of PEI modified MNPs and FITC labeling

In the present study, magnetic γ-Fe_2O_3 nanoparticles (MNPs) were synthesized as superparamagnetic carrier cores through the chemical coprecipitation method,[36, 37] and more information about synthesis of γ-Fe_2O_3 nanoparticles are provided in the Supplementary Information (SI). As magnetic nanocarriers in this study, the PEI-MNPs were synthesized

through electrostatic adsorption, which involved a two-step reaction, i.e., synthesis of core magnetic γ-Fe_2O_3 nanoparticles and the conjugation of MNPs with PEI. The preparation of MNPs followed the previously reported protocol with minor modifications.[36, 37] Aqueous PEI solution were subsequently added to MNPs solution (W:W=1:2), magnetically stirred for 24 h. Then the PEI-MNPs were washed three times under magnetic field using DI water. PEI-MNPs were finally suspended in DI water and stored at 4 ℃ until use.

To visualize dynamic change of PEI-MNPs in glioblastoma U251 cells, the PEI-MNPs were fluorescently labeled with fluorescein isothiocyanate (FITC).[38] Firstly, 100 mg of PEI-MNPs were resuspended in 10 mL of borate buffered saline (pH 8.4) and mixed with a solution of 100 μg/mL FITC solution. Following that the suspension was incubated 2 h with a low stirring at room temperature in the dark. Then, the FITC conjugated PEI-MNPs were washed three times under magnetic field using phosphate buffered saline (PBS, pH 7.4). The FITC-conjugated fluorescent PEI-MNPs (FITC-PEI-MNPs) were finally suspended in RPMI 1640 medium and stored at 4 □ until use. The FITC-PEI-MNPs were observed with an inverted fluorescence microscope (Eclipse TE 2000-U, Nikon, Kyoto, Japan) equipped with a high-resolution CCD camera (CV-S3200, JAI Co., Japan).

2.4 Evaluation of biological properties of PEI-MNPs

The biological effects of PEI-MNPs on glioblastoma cells, including cellular uptake, cell viability, cytotoxicity, and apoptosis were evaluated before using them as carries for siRNA delivery. More information was provided in the Supplementary Information (SI).

2.5 Intracellular imaging of FITC-PEI-MNPs in U251 cells

Intracellular internalization of FITC-PEI-MNPs in U251 glioblastoma cells was then

performed by co-culturing U251 cells with the FITC labeling PEI-MNPs. Briefly, the U251 cells were seeded in 24-well plates and cultured for 48 h, and then the FITC-labeling PEI-MNPs (80 μg/mL, diluted using RPMI 1640 medium) were added to the U251 cells. After incubation for 4 h, the culture medium and the residual FITC-labeling were then replaced and washed three times with PBS, and then were immunofluorescent stained by rhodamine conjugated phallodim, the cells were counterstained with DAPI dye (100 nM; Sigma-Aldrich) to reveal nuclei. The prepared samples were observed under an inverted fluorescence microscope (Eclipse TE 2000-U, Nikon, Kyoto, Japan) equipped with a high-resolution CCD camera (CV-S3200, JAI Co., Japan).

2.6 Preparation of siRNA~PEI-MNPs

The binding ability of PEI-MNPs with siRNA was performed by ultraviolet-visible spectrophotometry and the gel retardation assay. To prepare siRNA binding with PEI-MNPs, 2 μL of synthesized survivin siRNA (37.8 pmol/μL) was mixed with PEI-MNPs with a series of weight (1, 4, 7, 10, 13 μg) in the DEPC-treated water, and was shaken for 15 min at 37℃, allowing for sufficient binding of siRNA molecules with the PEI-MNPs. The formed siRNA~PEI-MNPs suspension was centrifuged, and then separated magnetically. The prepared supernatant was analyzed by ultraviolet-visible spectrophotometer (NanoDrop 2000, themro) at A260 nm to reveal siRNA content. Meanwhile, the siRNA~PEI-MNPs were loaded onto 2% agarose gel for electrophoresis in TAE buffer at a constant voltage of 100 V for 10 min, and the agarose gel was then stained with the 0.5 μg/ml ethidium bromide solution for 15 min to visualize the siRNA bands using a UV gel image system (InGenius LHR, SynGene, UK).

2.7 Serum stability of siRNA~ PEI-MNPs

To estimate the stability of siRNA against nuclease attack in serum, the naked siRNA and siRNA~PEI-MNPs loaded with 8 μL of survivin siRNA (20 μM) solution were incubated at 37℃ in 20 μL of DEPC water containing 50% (v/v) fetal bovine serum (FBS). At each predetermined time point, the mixtures were treated with 20 μL of heparin sodium salt solution (25 mg/mL) for 15 min, and then analyzed by 2% agarose gel electrophoresis at 40 V for 20 min.

2.8 Cellular uptake of siRNA~PEI-MNPs

The cellular uptake of survivin siRNA~PEI-MNPs was assayed by co-culturing glioblastoma U251 cells with the FAM labeling siRNA~PEI-MNPs. Briefly, the U251 cells were seeded into a 24-well plate at a density of 5 x 10^4 cells/well in 600 μL of culture medium, and cultured for 24h.Subsequently, the FAM-labeled siRNA was loaded onto PEI-MNPs, to form the FAM labeling siRNA~PEI-MNPs, which were then added into the wells seeded with the U251 cells and incubated for 4 h. The sample was then replaced and rinsed by PBS to remove residual siRNA~PEI-MNP, and fixed with freshly prepared 2% formaldehyde solution. The cellular uptake of the siRNA~PEI-MNPs were determine by a FACS Calibur flow cytometer (BD Biosciences, San Jose, CA), and analyzed using CELLQUEST software (BD Biosciences). At the same time, the cellular uptake of siRNA~PEI-MNPs was also evaluated by fluorescence microscopy (Eclipse TE 2000-U, Nikon, Japan) equipped with a high-resolution CCD camera (CV-S3200, JAI Co., Japan), after that the cells were counterstained with DAPI (100 nM; Sigma-Aldrich) to reveal nuclei.

2.9 Assay of cell proliferation capacity and cell viability

To evaluate anti-proliferation capacity of survivin siRNA~PEI-MNPs, The 3-(4, 5)-dimethylth-iahiazo(-z-y1)-3,5-diphenytetrazoliumromide (MTT) assay was used to evaluate cell proliferation on the treated U251 cells. Briefly, 10 μL of the survivin siRNA~PEI-MNPs solution were added to the microwell plates that were seeded with U251 cells at a density of 1×10^4 cells/well, and then incubated for 6 h. The fresh culture medium was then added and incubated for another 42 h. 200 μL of the MTT solution (final concentration: 0.5 mg/mL; Sigma-Aldrich Co.) was then added and incubated for 4 h, and 150 μL of dimethyl sulfoxide (DMSO) was successively added and incubated for another 15 min. Finally the absorbance of the sample was measured at 570 nm on a microplate spctrophotometer (Bio Tek Instrument Inc., USA).

The cell viability of the treated glioblastoma U251 cells was assessed using a fluorescein diacetate (FDA) and propidium iodide (PI) double-staining protocol.[39, 40] The U251 cells of proper growth stage were seeded at a density of 2×10^4 cells/well, and 100 μL of the survivin siRNA~PEI-MNPs solution were added and incubated for 6 h. The fresh culture medium was added and co-cultured for another 42 h. Subsequently, the FDA solution (final concentration: 1 μg/mL) and PI solution (final concentration: 20 μg/mL) were successively introduced into the culture plates, and then incubated for 10 min at room temperature. The living cells were stained green by FDA, whereas the dead cells were stained red by fluorescent dye PI. The cell viability was then estimated by counting the live and the dead cells under an inverted fluorescence microscope (Eclipse TE 2000-U, Nikon, Kyoto, Japan) equipped with a high-resolution CCD camera (CV-S3200, JAI Co., Japan).

2.10 Cell cycle analysis

The cell cycle of the treated U251 cells was analyzed using flow cytometry. In brief, The U251 cells were firstly treated with survivin siRNA~PEI-MNPs as described above. The treated cells were then harvested and dissociated into a single-cell suspension in 500 μL PBS, and fixed by adding 2 mL of 70% ice-cold ethanol, followed with incubation at 4℃ overnight. The prepared cell suspension was then centrifuged to discard the fixative, resuspended in 2 mL of PBS solution, and filtered using a 200 mesh cell screen. The pelleted cells were resuspended in 1 mL of 50 μg/mL PI solution containing 20 μg/mL RNase for cell staining. The cells were incubated in the dark for 1 h at 4 ℃, and analysed using a FACS Calibur flow cytometer (BD Biosciences, San Jose, CA), and analyzed using CELLQUEST software (BD Biosciences).

2.11 Apoptosis assay

Fluorescence Hoechst H33258 staining of apoptotic cells was performed to visualize apoptotic cells. Briefly, the treated U251 cells were fixed with 4% paraformaldehyde for 15 min, washed thrice with PBS, and then stained with bisbenzimide dye Hoechst H33258 solution (2 μg/mL) for 10 min at room temperature. The stained cells were rinsed thrice with PBS and observed using an inverted fluorescence microscope (Eclipse TE 2000-U) equipped with a high-resolution CCD camera (CV-S3200).

2.12 Detection of nuclear DNA fragmentation

The treated U251 cells were harvested using 0.25% trypsin without EDTA and washed twice with PBS (pH 7.4), and then suspended in 100 μL lysis buffer and mixed vigorously for 10 s. The samples were centrifuged at 1,000 × *g* for 5 min to obtain the supernatants, which were subsequently mixed with 500 μL CTAB (0.1% *β*-mercaptoethanol) and incubated for 1 h at

65 ℃. In each tube was added an equal volume of phenol-chloroform-isoamyl alcohol, centrifuged for 10 min after mixing (12,000 × *g*). The supernatant was transferred and added with an equal volume of chloroform-isoamyl alcohol, centrifuged for 10 min after mixing (12,000 × *g*). The obtained supernatant was transferred again and added with an equal volume of isopropanol to precipitate DNA after incubation at 4 ℃ for 6 h. the DNA precipitate was obtained by centrifugation for 15 min (12,000 × *g*). 500 μL TE was added to resuspend the precipitate to obtain aqueous DNA solution, which was then added with the RNA enzyme and incubated for 1 h at 37 ℃. Finally, a DNA pellet was obtained by centrifugation at 12,000 × *g* for 20 min. The white DNA pellet was washed twice with 500 μL 70% ice-cold ethanol, air-dried at room temperature, and dissolved in 50 μL TE buffer. The DNA fragments were analyzed by electrophoresis with 1.5% agarose gel and visualized under ultraviolet illumination after staining with ethidium bromide.

2.13 Autophagy assay

The volume of acidic vesicular organelles (AVOs), as a marker of autophagy, was detected by staining with lysosomotropic agent acridine orange (AO). The cytoplasm and nucleus of the stained cells fluoresced bright green, whereas the AVOs fluoresced bright red. The treated cells were stained with AO (5 μg/mL) at 37℃for 1 min and observed by inverted fluorescence microscope (Eclipse TE 2000-U) equipped with a high-resolution CCD camera (CV-S3200).

Immunocytochemistry staining was used to detect the autophagy marker LC3. The treated U251 cells were then fixed with 4% paraformaldehyde for 30 min at room temperature after washing with PBS thrice. Triton X-100 (0.1%) solution was then used to permeabilize the cells for another 30 min at room temperature. The permeabilized cells were then incubated

with 5% newborn calf serum in PBS for 30 min at 37 ℃ to block nonspecific binding for immunocytochemistry staining. The cells were incubated overnight in sequence at 4 ℃ with anti-LC3A/B antibody (mouse monoclonal IgG1, 1:100). After rinsing with PBS thrice, the PBS-diluted fluorescence-labeled secondary Alexa Fluor 488 goat anti-mouse IgG (1:20) were applied for the treated cells and incubated at 37 ℃ for 1 h. The cell nuclei were counterstained with DAPI dye (100 nM; Sigma-Aldrich) to reveal the nuclei.

2.14 LC3-Ⅱ expression assay by qRT-PCR analysis

To quantitatively determine the level of mRNA expression of LC3-II, total RNA was extracted from treated U251 cells using the TRIzol reagent (Invitrogen, America) according to the manufacturer's instructions. A total of 1 μg of RNA was transcribed into cDNA using random primers and M-MLV reverse transcriptase (Promega). The qRT-PCR was performed in a final volume of 20 μl containing 10 μl of SYBR GREEN, and 2 μL of each 10 μM primer, and 1 μL cDNA products. The amplification program was performed with one cycle at 95°C for 3 min, followed by 32 cycles at 95°C for 30 sec, at 65°C for 30 sec, and at 72°C for 1 min, and finally at 72°C for 5 min. After amplification, a melting curve analysis was performed by collecting fluorescence data. GAPDH was used as the control in this study. The primers for GAPDH: Fwd-5′-CCACCCATGGCAAATTCCATGGCA-3′, Rev-5′-TCTATCTAGACGGCA GGTCAGGTCCACC-3′, LC3-II: Fwd-5′- GAGAAGCAGCTTCCTGTTCTGG-3′, Rev-5′-GTGTCCGTTCACCAACAGGAAG-3′. All samples were performed at least with three biological replicates.

2.15 Characterization methods

A transmission electron microscope (TEM, JEM-2100, Japan) were employed to characterize

the morphology and size of the prepared magnetic γ-Fe_2O_3 nanoparticles (MNPs) and PEI-MNPs. The crystal structure of MNPs and PEI-MNPs was analyzed with an X-ray diffractometer (XRD, Philips D/Max-2500, Holland) using a monochromatic X-ray beam with nickel-filtered Cu-Kα radiation. Fourier transform infrared spectroscopy (FT-IR, Nicolet NEXUS 670, USA) was performed to record the FT-IR spectra of the MNPs and PEI-MNPs. Dried samples were pressed with KBr powder into pellets. Sixty-four scans were signal-averaged in the range from 4000 to 400 cm^{-1} at a resolution of 4 cm^{-1}. Their magnetic measurements were carried out on a vibrating sample magnetometer (LAKESHORE-7304, USA) by changing H between +1375 and −1375Oe. Fluorescence images were photographed using an inverted fluorescence microscope (Eclipse TE 2000-U, Nikon, Kyoto, Japan) equipped with a high-resolution CCD camera (CV-S3200, JAI Co., Japan). The cell cycle and cellular uptake were analyzed using FACS Calibur flow cytometer (BD Biosciences, San Jose, CA).

2.16 Image acquisition and analysis

Bright-field and fluorescence images were acquired using an inverted fluorescence microscope (Eclipse TE 2000-U, Nikon, Kyoto, Japan) equipped with a CCD camera (CV-S3200, JAI Co., Japan). Software Image-Pro Plus® 6.0 (Media Cyternetics) and SPSS 12.0 (SPSS Inc.) were used to perform image analysis and statistical data analysis, respectively. The quantitative data are presented as means ± standard deviation (SD) for each experiment. All experiments were performed with three replicates, and the results presented were from representative experiments.

3 Results and discussion

3.1 Synthesis and characterization of MNPs and PEI-MNPs

In the present study, magnetic γ-Fe_2O_3 nanoparticles (MNPs) were synthesized as superparamagnetic carrier cores through the chemical coprecipitation method.[36, 37] The PEI-MNPs preparation was performed via a two-step process including synthesis of magnetic γ-Fe_2O_3 nanoparticles (MNPs) and PEI encapsulation by electrostatic adsorption method, and subsequently, the morphology and performance of as-prepared PEI-MNPs were characterized. As shown in Figure 2, the TEM images showed that the nano-sized particles were obtained and had a uniform morphology. The prepared MNPs showed a rather narrow size distribution, and the diameter of a single particle ranged in size from 10 nm to 15 nm (Figure 2 A), and the PEI surface-coating of the MNPs did not obviously affect the morphology and size of the iron oxide crystallites obviously (Figure 2 B),and the size distribution of the tested MNPs and PEI-MNPs nanoparticles was also similar (Figure S1, SI). Meantime, the X-ray powder diffraction (XRD) pattern showed six characteristic peaks marked with the indices (220), (311), (400), (422), (511), and (440) were observed for the MNPs and PEI-MNPs, which distinctly match standard γ-Fe_2O_3 reflections, and clearly show that the incorporation of PEI to MNPs does not influence γ-Fe_2O_3 crystallization (Figure 2C). The composition of the PEI-MNPs was analyzed by FT-IR spectroscopy. As illustrated in Figure 2 (D), the characteristic band (Fe-O) of MNPs was situated at 596.6 cm^{-1}, and the peaks at 1558 and 1647 cm^{-1} were attributed to the characteristic band of PEI, and the data confirmed that the MNPs were successfully modified by PEI with altered characteristic band.

The Figure 2 (E) illustrated that the magnetization curve of the prepared PEI-MNPs

appeared a symmetrical hysteresis loop that was also observed within MNPs (Figure S2, SI) and this featured loop indicates that the PEI-MNPs are readily magnetized in the presence of a magnetic field and the removal of the magnetic field results in minimal residual magnetization within the particles in different medium (including DI water, RPMI 1640, PBS (pH 7.4)) (F). Moreover, the saturation magnetization of the prepared PEI-MNPs was 22.75 emu/g, which assured that the prepared PEI-MNPs could be widely applied in biomedical fields. Besides, we examined the zeta potential of the prepared MNPs and PEI-MNPs. The data showed the PEI-MNPs were positively charged at around +14.6 mV, in comparison with the naked MNPs that were negatively charged at around -19.6 mV (SI, Figure S3).

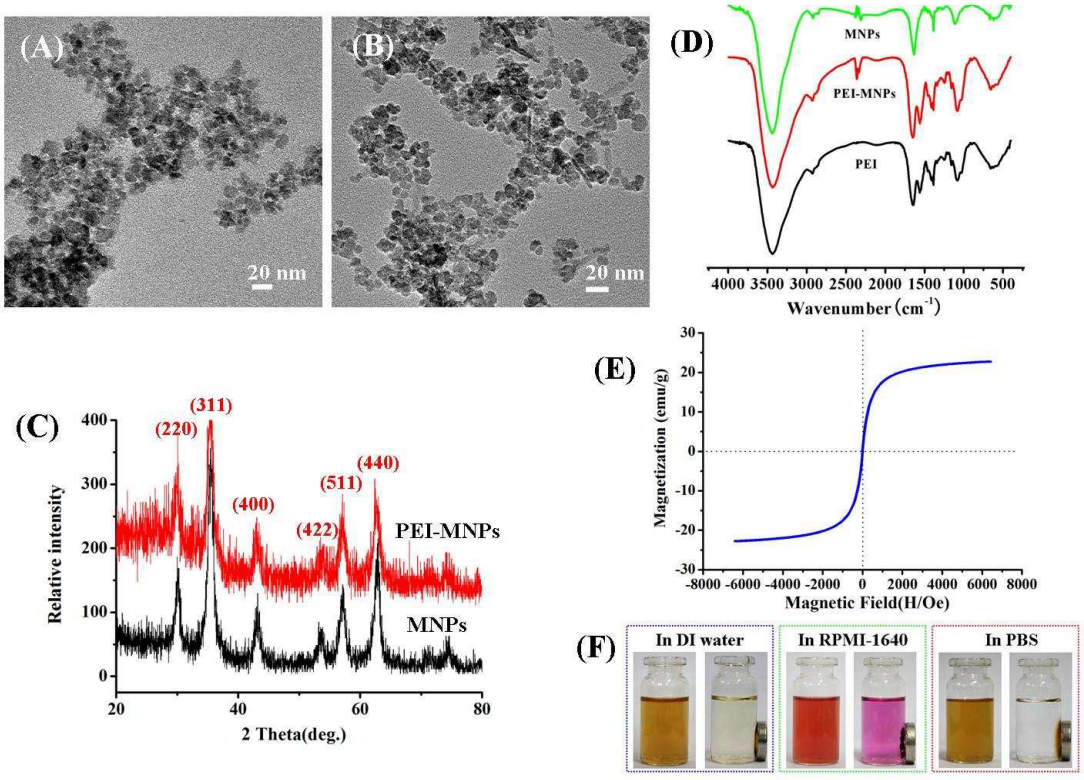

Figure 2 Characteristics of magnetic γ-Fe_2O_3 nanoparticles (MNPs). TEM observation for MNPs (A, 800 00 × magnification) and PEI-MNPs (B, 800 00 × magnification). (C) XRD

pattern of MNPs (black) and PEI-MNPs (red). (D) FT-IR spectra of MNPs, PEI-MNPs and PEI. (E) The magnetic hysteresis loop of PEI-MNPs at 300 K. (F) The response to an external magnetic field by adding and removing an external magnetic field in different medium.

3.2 Cytotoxicity and cell viability of PEI-MNPs

The cytotoxicity of the prepared PEI-MNPs was analyzed for the treated cells with the MTT assay, which is a commonly used method to evaluate cytotoxicity.[41, 42] In this assay, MTT, a yellow tetrazole, is reduced into a purple formazan in living cells, which depends on NAD(P)H-dependent oxidoreductase enzymes found largely in the cytosolic compartment of the cell.[43, 44] Therefore, the U251 cells were incubated with the PEI-MNPs dispersion of different concentrations from 5 to 80 μg/mL for 48 h. The results indicated that the treated U251 cells generally exhibited a comparable proliferation activity in contrast with the untreated cells (Figure 3 A). Likewise, a negligible cytotoxicity of the PEI-MNPs with a concentration less than 80 μg/mL was also reconfirmed by cell viability and apoptosis assay (Figure S5 & S6, SI). Therefore, these data indicated that the fabricated PEI-MNPs could serve as a vehicle for siRNA delivery towards U251 cells.

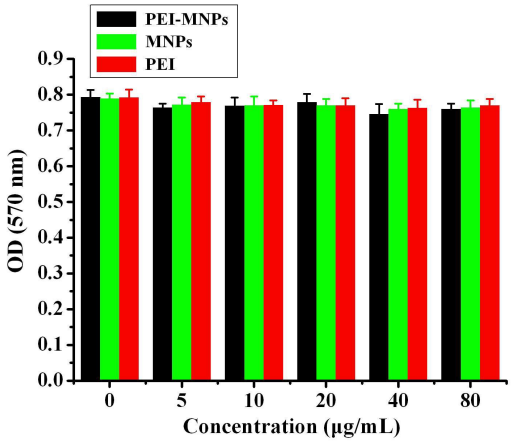

Figure 3 The growth ability of treated U251 cells with PEI-MNPs.

3.3 Intracellular imaging of PEI-MNPs in U251 glioblastoma cells

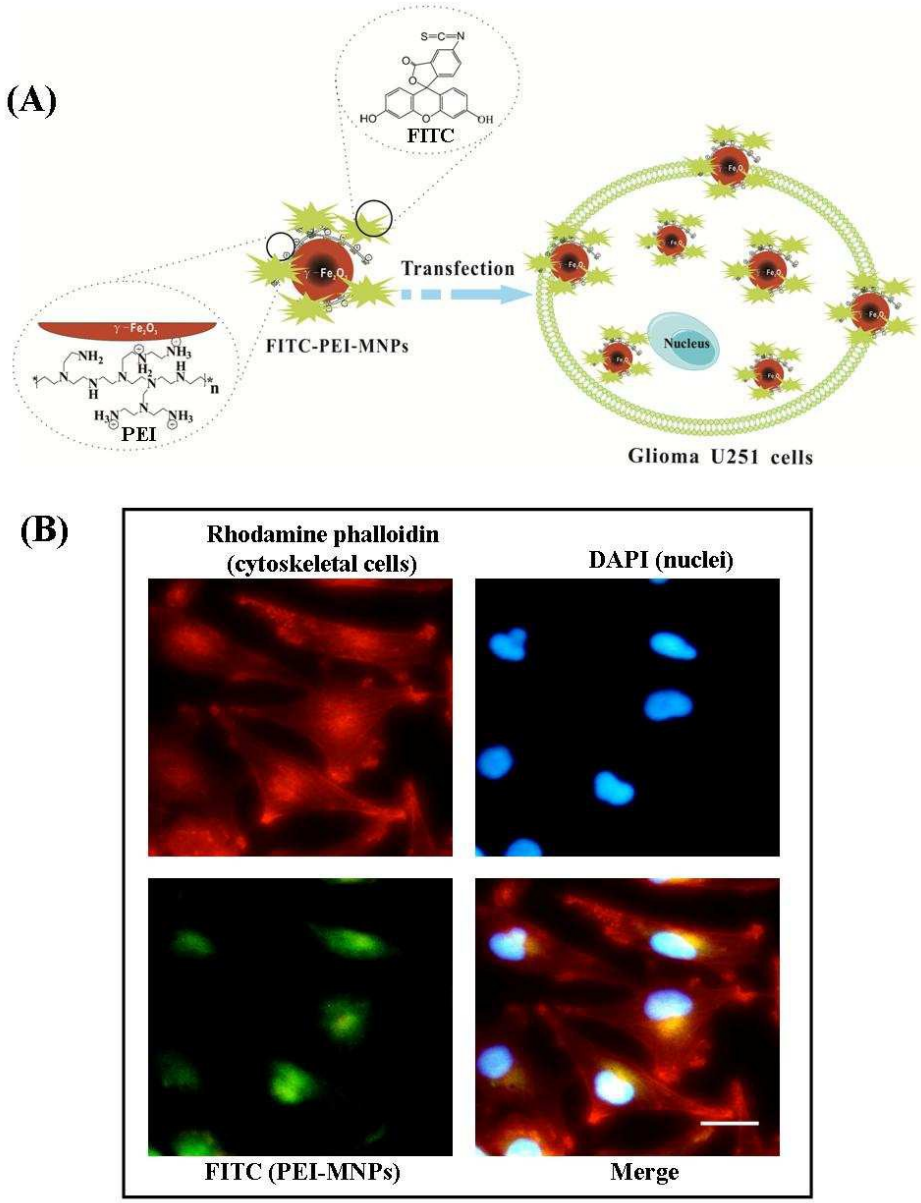

Figure 4 Intracellular imaging of the FITC-labeling PEI-MNPs in the U251 cells. Schematic diagram (A). Experimental images (B) of the U251 cells incubated with fluorescent FITC-labeling PEI-MNPs, the skeletal cells were revealed by phalloidin and nuclei were stained with DAPI. Scale bar = 50 μm.

Intracellular imaging of PEI-MNPs designed as in figure 4A, was performed by incubating the fluorescent FITC-labeling PEI-MNPs with U251 cells for 4 h. The results showed the FITC-labeling PEI-MNPs could effectively enter into cells and approach the nuclei, as the green fluorescence labeled PEI-MNPs were revealed close to nuclei within the treated cells (Figure 4 B). These results suggested that PEI-MNPs could be a potential vehicle for siRNA delivery towards U251 cells.

3.4 siRNA binding ability and serum stability assay

The positively charged PEI-MNPs with a cationic shell layer were expected to function with anionic siRNA by electrostatic interactions. Gel retardation was performed to evaluate binding ability of siRNA molecules with PEI-MNPs, and the unbinding siRNA molecules kept in the supernatant were detected using ultraviolet-visible spectrophotometry to estimate the binding siRNA with PEI-MNPs. As shown in Figure 5A, the amount of binding siRNA molecules increased with more PEI-MNPs used, and the free siRNA molecules detected simultaneously reduced. Gel retardation also showed that the residual free siRNA molecules were reduced and hardly detected as more coupling with increasing amount of PEI-MNPs applied (Figure 5 B).

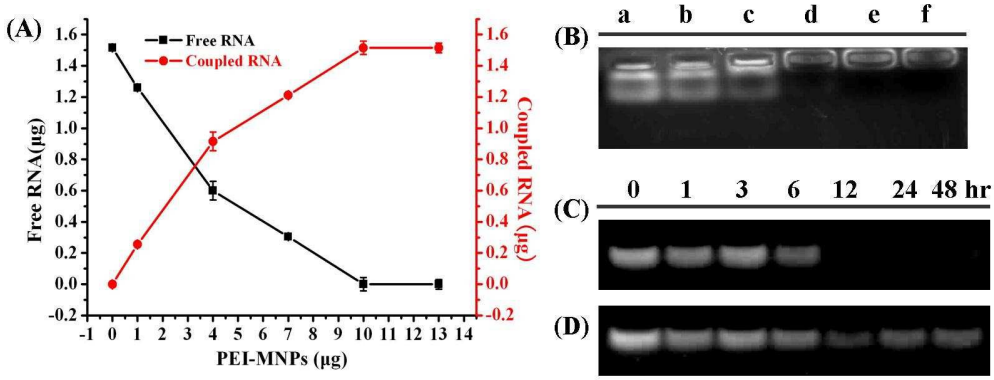

Figure 5 Binding capacity and stability of siRNA molecules coupled with PEI-MNPs. The dynamic change of siRNA molecules binding with PEI-MNPs (A). Gel retardation assay of siRNA~PEI-MNPs with different weight ratio of PEI-MNPs to siRNA (B), the lanes from left to right represented the free siRNA (a, control) and bound siRNA with PEI-MNPs with different weight of 1 μg (b), 4 μg (c), 7 μg (d), 10 μg (e), and 13 μg (f) respectively, which indicated an effective binding ability between siRNA and PEI-MNPs. Serum stability of free siRNA (C, control) and siRNA~PEI-MNPs (D) detected in DEPC water containing 50% (v/v) FBS after incubation for hours.

The serum stability of siRNA coupled with PEI-MNPs was tested in DEPC water containing 50% serum at 37 °C. the results showed that the naked siRNA was completely degraded after treatment for 6 h (Figure 5 C), but degradation of the coupled siRNA with PEI-MNPs was much slower than that of naked siRNA，and a substantial amount of siRNA molecules was still detected after incubation for 48 h (Figure 5 D). These results indicated that the PEI-MNPs could effectively protect siRNA from degradation by celluar nucleases, which thus may lead to improved cellular association and enhanced transfection efficiency.

3.5 Uptaking efficiency of siRNA~PEI-MNPs in U251 cells

The efficiency of cellular uptaking seriously affected gene delivery by nanocarriers in the transfection process for non-viral vector.[45, 46] The poor cellular uptake usually results in the low amount of intracellular siRNA, and leads to the low efficiency of RNA interference. So, we examined cellular uptake behaviors of the PEI-MNPs by flow cytometry and an inverted fluorescence microscope to reveal their effectiveness for siRNA delivery to U251 cells. The FAM-labeled siRNA~PEI-MNPs were used to treat U251 cells and evaluate their cellular

uptaking. As shown in Figure 6, the flow cytometric data showed that the U251 cells could efficiently uptake the siRNA~PEI-MNPs, and the uptake efficiency of siRNA~PEI-MNPs was higher than that of naked siRNA, which demonstrated that the delivery potential of PEI-MNPs. Besides, as demonstrated by fluorescence microscope analysis (Figure S7, SI), the uptaking U251 cells displayed strong green fluorescence within the cytoplasm when they "swallowed" more siRNA~PEI-MNPs. Thus these results revealed that the fabricated PEI-MNPs could effectively deliver siRNA into U251 cells.

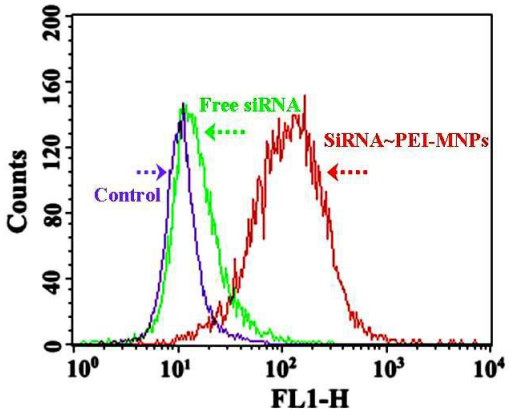

Figure 6 Uptaking measurement of siRNA~PEI-MNPs by U251 cells. The purple curve represented blank control (cells without treatment), and the green showed cells treated with free siRNA, and the red represented cells treated with siRNA~PEI-MNPs indicating an efficient cellular uptaking.

3.6 Anti-proliferation capability and cell viability assay

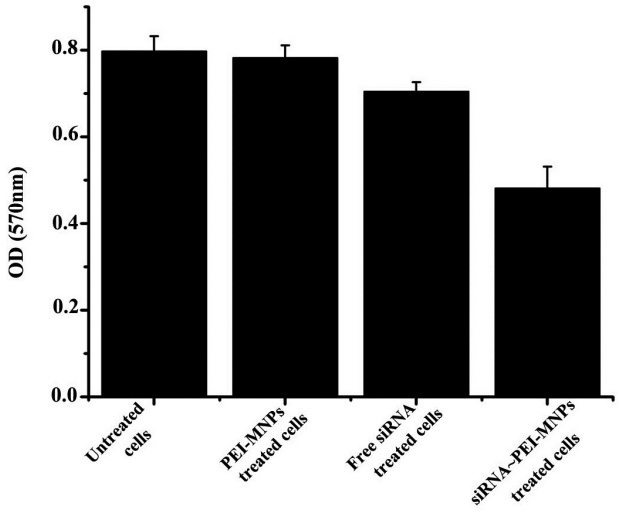

Figure 7 The growth ability of siRNA~PEI-MNPs treated U251 cells.

Anti-proliferation capacity of siRNA~PEI-MNPs treated U251 cells was evaluated by MTT assay, and the results demonstrated that cell proliferation capacity was greatly reduced after siRNA~PEI-MNPs treatment in comparison with untreated U251 cells and cells treated with free siRNA (Figure 7).

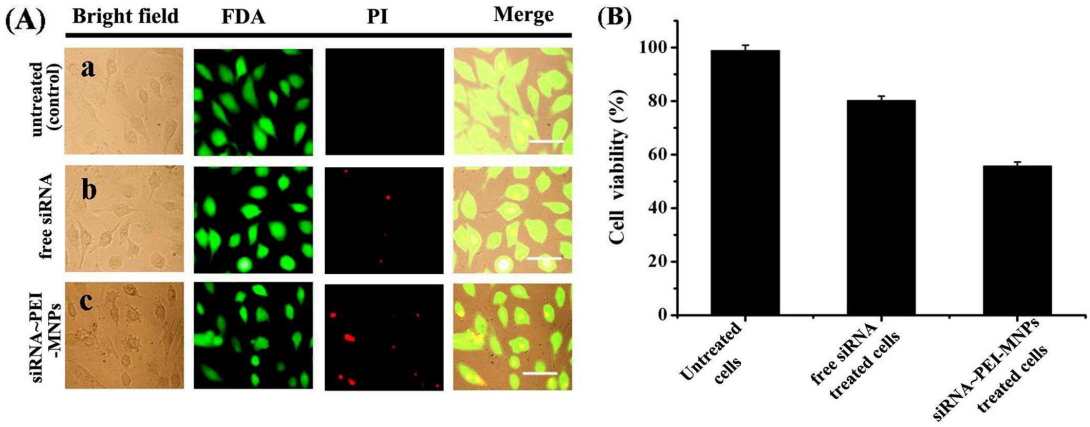

Figure 8 Cell viability detection and measurement of the treated U251 cells. The untreated cells were used as controls, and in comparison with cells treated with free siRNA, more dying cells were observed after the siRNA~PEI-MNPs treatment. Quantitative analysis was

performed by counting at least 500 cells with three replicates. Scale bar = 100 μm.

In addition, the PI and FDA double-staining was used to evaluate the viability of siRNA~PEI-MNPs treated U251 cells. PI is a DNA-binding fluorescent dye that only enters dead or dying cells with damaged or leaky membranes, producing red fluorescence, which thus has been used as a marker for apoptotic and necrotic cells.[39, 40] On the other hand, FDA, which stains cells with intact membranes, produces a bright green fluorescence.[39, 40] As shown in Figure 8 A compared with untreated cells (Figure 8a), the free siRNA treatment could not obviously produce dying cells, and most cells retained intact (Figure 8b). In contrast, the dying cells were obviously observed after siRNA~PEI-MNPs treatment (Figure 8c). Quantitative analysis shows that cell viability (65.6%) treated by siRNA~PEI-MNPs obviously decreases compared with untreated U251 cells (98.9%) (Figure 8 B). However, the cells with free siRNA treatment still had higher viability (80.2%). Therefore, the results indicated that the survivin siRNA~PEI-MNPs could effectively prevent cell proliferation and lead to death in tumor U251 cells.

3.7 Cell cycle analysis of siRNA~PEI-MNPs treated cells

The cell cycle of the U251 cells was analyzed after siRNA~PEI-MNPs treatment, and as shown in Figure 9，the data showed that the ratio of G2/M phase was about 12.35% in the untreated cells, 12.20% in PEI-MNPs, and 13.06% in free siRNA treatment cells respectively (Figure 9 A-C), but G2/M phase was about 38.55% in the siRNA~PEI-MNPs treated cells (Figure 9 D). The results indicated that siRNA~PEI-MNPs treatment could obviously affect cell cycle distribution and arrest cell cycle mostly at G2/M phase in the treated U251 cells.

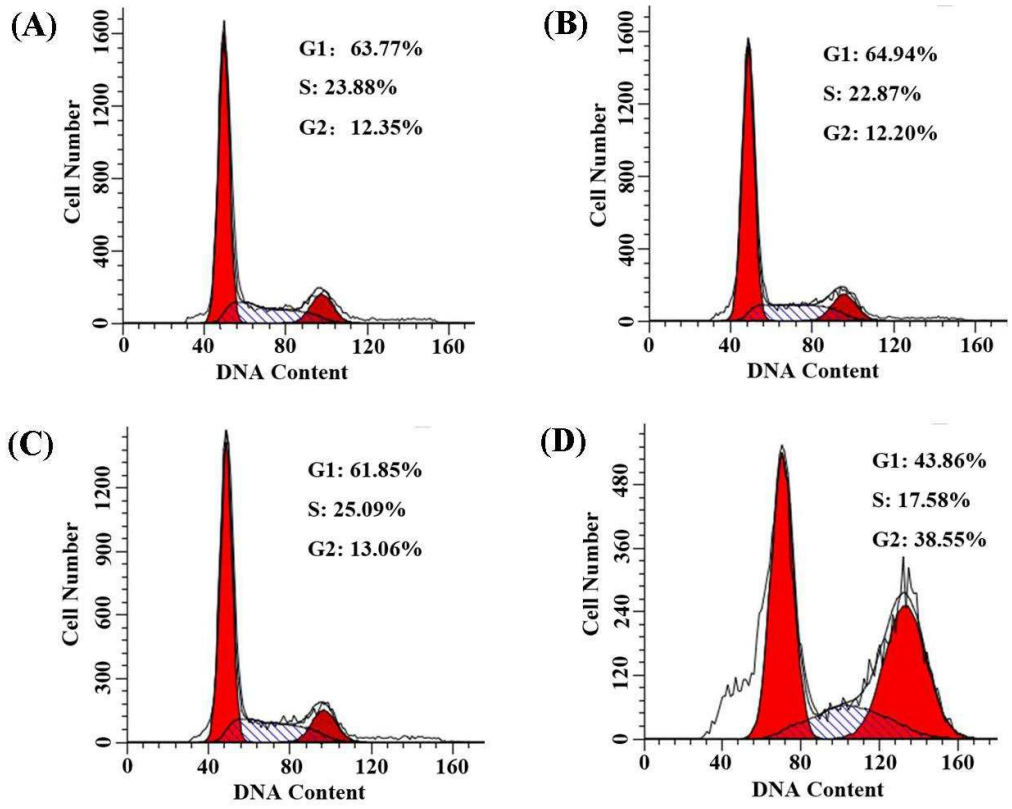

Figure 9. Cell cycle distribution of the treated U251 cells. The untreated U251 cells (A, controls), the PEI-MNPs treated cells (B), the free siRNA treated U251 cells (C), and siRNA~PEI-MNPs treated U251 cells (D).

3.8 Apoptosis and autophagy in siRNA~PEI-MNPs treated cells

Cell apoptosis is a process of programmed cell death. However, tumor cells are generally characterized by their ability to bypass apoptosis. Thus, apoptosis is commonly used as a hallmark of the improved treatment for targeted tumor cells in therapy, which is generally characterized with distinct morphological changes including chromatin condensation, and nuclear DNA fragmentation.[49, 50]

To reveal the chromatin condensation, the nuclear DNA content of treated cells was relatively quantified with fluorescence intensity by nuclear dye Hoechst H33258, which binds

to AT-rich regions of nuclear DNA and allows detection and relative quantification of the DNA of apoptotic cells.[51, 52] As shown in Figure10 A (top), the siRNA~PEI-MNPs treated U251 cells displayed a much more bright and condensed chromatin, in contrast with cells treated with free siRNA and PEI-MNPs repectively. Figure 10 A (bottom) showed apoptotic analysis of treated U251 cells, and statistically the apoptosis rate of the siRNA~PEI-MNPs treated U251 cells was about 59.5%, significantly higher than the cells treated with free siRNA (21.4%). Besides，nuclear DNA fragmentation as a hallmark of apoptosis cells was also analyzed, as DNA breakage by Ca^{2+}- and Mg^{2+}- dependent endonucleases occurs during apoptosis, eventually resulting in DNA fragments of 180 to 200 base pairs.[53, 54] As shown in figure 10 B, the DNA laddering assay demonstrated that fragmented DNA were clearly observed in the siRNA~PEI-MNPs treated U251 cells in contrast with that in free siRNA treated U251 cells. Taken together, these results indicated that siRNA~PEI-MNPs could obviously induce apoptosis in the U251 cells.

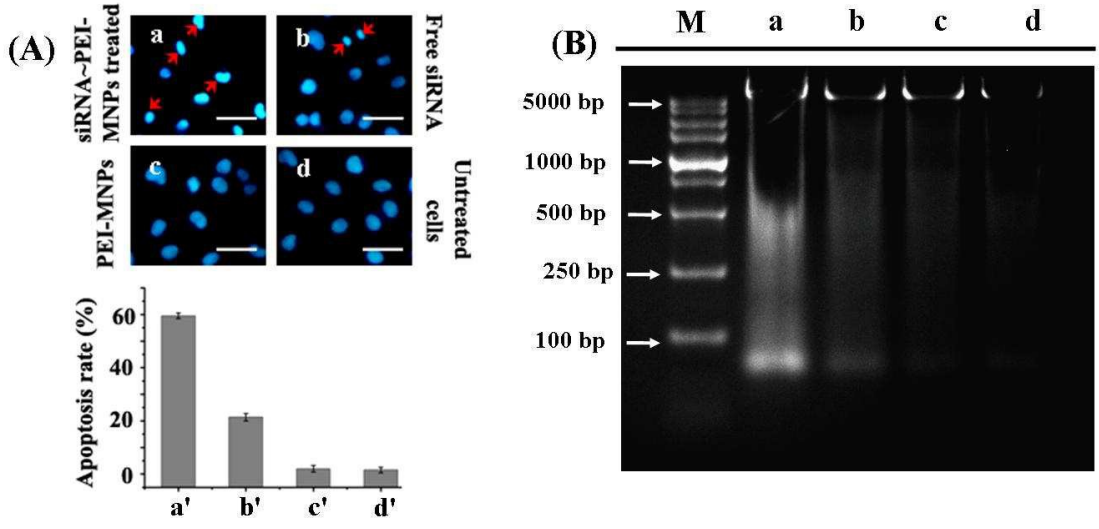

Figure 10 Hoechst staining and apoptotic DNA laddering in the treated U251 cells. (A) The

siRNA~PEI-MNPs treated U251 cells produced much condensed and overbright nuclei (top, a), in contrast with cells treated with the free siRNA (top, b), and PEI-MNPs (top, c), and the untreated U251 cells were used as controls (top, d), (B) the apoptotic analysis of cells treated with siRNA~PEI-MNPs (bottom, a′), free siRNA (bottom, b′), and PEI-MNPs (bottom, c′), and untreated cells as controls (bottom, d′). Scale bar = 100 μm. Accordingly, (B) in the apoptotic DNA laddering assaying, the siRNA~PEI-MNPs treated U251 cells yielded more DNA fragments (B, a), in comparison with cells treated with the free siRNA (B, b), and PEI-MNPs (B, c), and untreated U251 cells were used as controls (B, d).

Autophagy is a process of bulk protein degradation through an autophagosomic- lysosomal pathway, which is initiated by the formation of autophagosomes [55, 56], and classified as programmed cell death type II.[57] During autophagosome formation, microtubule associated protein light chain 3 I (LC3-I) is conjugated to phosphatidylamine to form LC3-phosphatidylamine (LC3-II). The production of LC3-II is an essential process during the formation of the autophagosome. Therefore, the ratio of LC3-II levels to LC3-I levels reflected the activation of autophagy, and the formation and promotion of acidic vesicular organelles (AVOs), as a characteristic of autophagy, could be detected by acridine orange (AO) staining [58, 59]. Moreover, the expression level of LC3-II mRNA was quantitatively determined by qRT-PCR in the treated U251 cells. As shown in Figure 11B, a remarkable increase of LC3-II mRNA expression level was detected in the siRNA~PEI-MNPs treated U251 cells compared with cells treated with free siRNA and PEI-MNPs respectively.

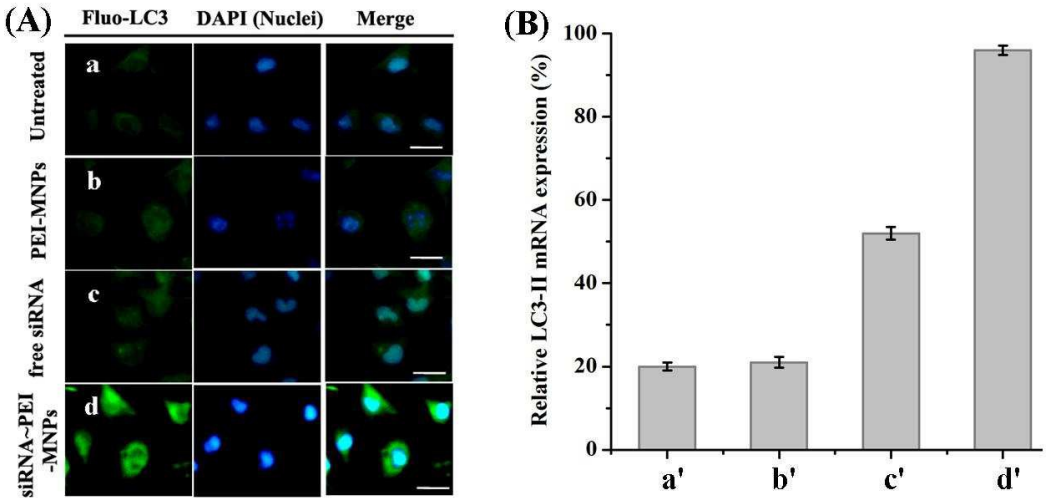

Figure 11 (A) Accumulated cytoplasmic LC3 signal as a hallmark of autophagy in treated U251 cells. The untreated U251 cells were used as controls (a), and in contrast with cells treated with PEI-MNPs (b), and free siRNA (c), the LC3 signal was obviously detected in siRNA~PEI-MNPs treated cells (d). Scale bar =100 μm. (B) QRT-PCR analysis of LC3-II mRNA expression level in the untreated U251 cells (a′), and cells treated with PEI-MNPs (b′), and free siRNA (c′), and siRNA~PEI-MNPs (d′).

The cytoplasmic protein LC3, as another hallmark of autophagy, was revealed by its anti-LC3A/B antibody. The siRNA~PEI-MNPs treated U251 cells were stained with immunocytochemistry and observed under a fluorescence microscopy, the results showed that the LC3 puncta were markedly accumulated in cytoplasm in the siRNA~PEI-MNPs treated cells (Figure 11). Therefore, these results suggested that siRNA~PEI-MNPs could induce autophagy in U251 cells. Besides, the siRNA~PEI-MNPs treated U251 cells were stained with AO, and the results showed that the acidic vesicular organelles (AVOs) formed in the treated cells as red fluorescent dots was observed in cytoplasm (Figure 12).

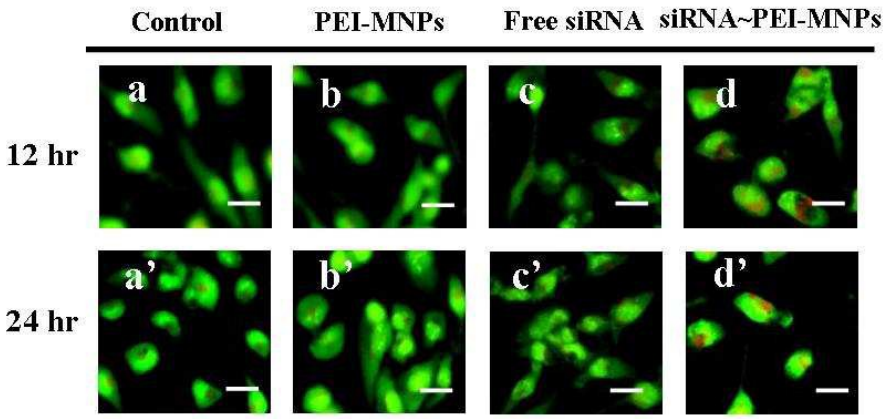

Figure 12. AO staining in the treated U251 cells. In contrast with the untreated U251 cells as controls (a & a'), no AO stain was obviously observed in the cells treated with PEI-MNPs (b & b') and free siRNA (c & c'), but staining was clearly detected in the siRNA~PEI-MNPs treated U251 cells for 12 h or 24 h (d & d') respectively. Scale bar =50 μm.

4 Conclusions

In the present study, we have attempted to develop PEI surface-modified MNPs as multipurpose nanocarriers for combined bioimaging, siRNA delivery for in vitro therapy of tumor cells. The fabricated PEI-MNPs having a cationic polymer shell could efficiently absorb adequate siRNA molecules via electrostatic interaction, and effectively protect them from enzymatic degradation in serum in vitro. The fluorescently labeled PEI-MNPs enabled to enter the tumor cells and gain access to nuclei precisely for intracellular imaging of siRNA delivery, and the constructed survivin siRNA~PEI-MNPs were successfully delivered into glioblastoma multiforme U251 cells, and effectively inhibited cell proliferation, induced apoptosis and autophagy of targeted U251 cells, which was confirmed by analysis of

biological activity in the treated tumor cells. Therefore, the present study demonstrated that the fabricated PEI-MNPs were a promising nanocarrier for intracellular imaging and siRNA delivery for in vitro therapy of glioblastoma multiforme via gene silencing of siRNA payloads.

Acknowledgments: This work was supported by the National Natural Science Foundation of China (No. 314 008 55), the Technological innovation incubator program from Henan University of Technology (No.201 518), the Introduced Postdoctoral Talents of Henan University of Technology (No.150 199), the Basal Research Fund of Henan University of Technology (No. 2014 YWQ Q15).

Appendix A. Supplementary data: Supplementary data associated with this article can be found in on-line attachments.

References

1 A. Behin, K. Hoang-Xuan, A.F. Carpentier and J.Y. Delattre, *Lancet*, 2003, **361**, 323-331.

2 R. Stupp, M.E. Hegi, M.R. Gilbert and A. Chakravarti, *J. Clin. Oncol.*, 2007, **25**, 4127-4136.

3 R. Stupp, M.E. Hegi, M.J. van den Bent, W.P. Mason, M. Weller, R.O. Mirimanoff and J.G. Cairncross, *Oncologist*, 2006, **11**, 165-180.

4 CBTRUS, Statistical Report, 1998-2002: Central Brain Tumor Registry of the United States. 2005.

5 P.Y. Wen and S. Kesari, *N. Engl. J. Med*., 2008, **359**, 492-507.

6 A.C. Mita, M.M. Mita, S.T. Nawrocki and F.J. Giles, *Clin. Cancer Res*., 2008, **14**, 5000-5005.

7 S.M. Kim, J.S. Woo, C.H. Jeong, C.H. Ryu, J.Y. Lim and S.S. Jeun, *Cancer Res*., 2012, **72**, 4807-4817.

8 P. Wang, H. Zhen, J. Zhang, W. Zhang, R. Zhang, X. Cheng, G. Guo, X. Mao, J. Wang and X. Zhang, *Mol. Carcinog*., 2012, **51**, 586-595.

9 X.F. Che, C.L. Zheng, S. Owatari, M. Mutoh, T. Gotanda, H.C. Jeung, T. Furukawa, R. Ikeda, M. Yamamoto, M. Haraguchi, N. Arima and S. Akiyama, *Blood*, 2006, **107** : 4880-4887.

10 Z. Medarova, W. Pham, C. Farrar, V. Petkova and A. Moore, *Nature medicine*, 2007, **13**, 372-377.

11 F. Yang, W. Huang, Y. Li, S. Liu, M. Jin, Y. Wang, L. Jia and Z. Gao, *Biomaterials*, 2013, **34**, 5689-5699.

12 J. Ellermeier, J. Wei, P. Duewell, S. Hoves, M.R. Stieg, T. Adunka, D. Noerenberg, H.J. Anders, D. Mayr, H. Poeck, G. Hartmann, S. Endres and M. Schnurr, *Cancer Res*., 2013,**73**, 1709-1720.

13 T. Fatemian, I. Othman and E.H. Chowdhury, *Drug Discov Today*, 2014, **19**, 71-78.

14 B.L. Davidson and P.B. McCray, *Nat Rev Genet*., 2011, **12**, 329-340.

15 B. Yu, S.H. Hsu, C. Zhou, X. Wang, M.C. Terp, Y. Wu, L. Teng, Y. Mao, F. Wang, W. Xue, S.T. Jacob, K. Ghoshal, R.J. Lee and L.J. Lee, *Biomaterials*, 2012, **33**, 5924-5934.

16 N. Tresilwised, P. Pithayanukul, P.S. Holm, U. Schillinger, C. Plank and O. Mykhaylyk, *Biomaterials*, 2012, **33**, 256-269.

17 J. Zhou, T.R. Patel, M. Fu, J.P. Bertram and W.M. Saltzman, *Biomaterials*, 2012, **33**, 583-591.

18 M. Kumar, M. Yigit, G. Dai, A. Moore and Z. Medarova, *Cancer Res*., 2010, **70**, 7553-7561.

19 K.A. Whitehead, R. Langer and D.G. Anderson, *Nat. Rev. Drug Discov.*, 2009, **8**, 129-138.

20 I. Posadas, F.J. Guerra and V. Ceña, *Nanomedicine*, 2010, **5**, 1219-1236.

21 F.C. Pérez-Martínez, J. Guerra, I. Posadas and V. Ceña, *Pharm. Res.*, 2011, **28**, 1843-1858.

22 K. Gao and L. Huang, *Mol. Pharm*., 2009, **6**, 651-658.

23 H. Katas and H.O. Alpar, *J. Control Release*, 2006, **115**, 216-225.

24 Y.K. Oh and T.G. Park, Adv. Drug. *Deliver. Rev*., 2009, **61**, 850-862.

25 L. Alvarez-Erviti, Y. Seow, H.F. Yin, C. Betts, S. Lakhal and M. J. Wood, *Nat. Biotechnol*., 2011, **29**, 341-345.

26 C.A. Hong and Y.S. Nam, *Theranostics*, 2014, **4**, 1211-1232.

27 S. Singh, *BioImpacts*, 2013, **3**, 53-65.

28 Y. Zhang, L. Arrington, D. Boardman, J. Davis, Y. Xu, K. DiFelice, S. Stirdivant, W. Wang, B. Budzik, J. Bawiec, J. Deng, G. Beutner, D. Seifried, M. Stanton, M. Gindy and A. Leone, *J. Control Release*, 2014, **174**, 7-14.

29 W. Tao, X. Mao, J.P. Davide, B. Ng, M. Cai, P.A. Burke, A.B. Sachs, and L. Sepp-Lorenzino, *Mol. Ther*., 2011, **19**, 567-575.

30 C.W. Evans, M. Fitzgerald, T.D. Clemons, M.J. House, B.S. Padman, J.A. Shaw, M. Saunders, A.R. Harvey, B. Zdyrko, I. Luzinov, G.A. Silva, S.A. Dunlop and K.S. Iyer, *ACS Nano*, 2011, **5**, 8640-8648.

31 J. Valencia-Serna, H. Gul-Uludağ, P. Mahdipoor, X. Jiang and H. Uludağ, *J. Control Release*, 2013, **172**, 495-503.

32 Y. Zhou, Z. Tang, C. Shi, S. Shi, Z. Qian and S. Zhou, *J. Mater. Sci. Mater. Med*., 2012, **23**, 2697-2708.

33 A. Akinc, M. Thomas, A.M. Klibanov and R. Langer, *J. Gene Med*., 2005, **7**, 657-663.

34 J.W. Park, K.H. Bae, C. Kim and T.G. Park, *Biomacromolecules*, 2011, **12**, 457-465.

35 K.H. Bae, K. Lee, J. Lee, I.S. Lee, J.H. Lee and T.G. Park, *J. Control Release*, 2011, **152**, e133-134.

36 S. Qu, H. Yang, D. Ren, S. Kan, G. Zou, D. Li and M. Li, *J. Colloid Interface Sci.*, 1999, **215**, 190-192.

37 Y.K. Sun, M. Ma, Y. Zhang and N. Gu, *Colloids Surf. A Physicochem Eng. Aspects*, 2004, **245**, 15-19.

38 X. Wang, F. Wei, S. Yan, H. Zhang, X. Tan, L. Zhang, G. Zhou, L. Cui, C. Li, L. Wang and Y. Li, *Biosens. Bioelectron*., 2014, **54**, 55-63.

39 B.W. Kristensen, H. Noer, J.B. Gramsbergen, J. Zimmer and J. Noraberg, *Brain Res*., 2003, **964**, 264-278.

40 X. Wang, L. Wang, X. Tan, H. Zhang and G. Sun, *J. Colloid Interface Sci*., 2014, **436C**, 267-275.

41 X. Lü, X. Bao, Y. Huang, Y. Qu, H. Lu and Z. Lu, *Biomaterials*, 2009, **30**, 141-148.

42 S. Mao, X. Shuai, F. Unger, M. Wittmar, X. Xie and T. Kissel, *Biomaterials*, 2005, **26**, 6343-6356.

43 S.J. Soenen, U. Himmelreich, N. Nuytten and M. De Cuyper, *Biomaterials*, 2011, **32**, 195-205.

44 S.J. Soenen, E. Illyes, D. Vercauteren, K. Braeckmans, Z. Majer, S.C. De Smedt and M. De Cuyper, *Biomaterials*, 2009, **30**, 6803-6813.

45 C.Y. Hsu and H. Uludağ, *Biomaterials*, 2012, **33**, 7834-7848.

46 M. Van der Aa, U.S. Huth, S.Y. Häfele, R. Schubert, R.S. Oosting, E. Mastrobattista, W.E. Hennink, R. Peschka-Süss, G.A. Koning and D.J. Crommelin, *Pharm. Res*., 2007, **24**,

1590-1598.

47 S.R. Denmeade and J.T. Isaacs, *Cancer Control*, 1996, **3**, 303-309.

48 S. Elmore, *Toxicol Pathol*., 2007, **35**, 495-516.

49 A.H. Koyama and Y. Miwa, *J. Virol*., 1997, **71**, 2567-2571.

50 A.H. Koyama and A. Adachi, *J, Gen. Virol*., 1997, **78**, 2909-2912.

51 K.F. Jorgenson, U. Varshney and J.H. van de Sande, *J. Biomol. Struct. Dyn*., 1988, **5**, 1005-1023.

52 S.Y. Breusegem, R.M. Clegg and F.G. Loontiens, *J. Mol. Biol*., 2002, **315**, 1049-1061.

53 C.D. Bortner, N.B. Oldenburg and J.A. Cidlowski, *Trends Cell Biol*., 1995, 5, 21-26.

54 Y. Higuchi, *J. Cell Mol. Med*., 2004, **8**, 455-464.

55 G. Kroemer and M. Jaattela, *Nat. Rev. Cancer*, 2005,**5**, 886-897.

56 T. Yorimitsu and D.J. Klionsky, *Cell Death Differ*., 2005, **12**, 1542-1552.

57 S. Shimizu, T. Kanaseki, N. Mizushima, T. Mizuta, S. Arakawa-Kobayashi, C. B. Thompson and Y. Tsujimoto, *Nat. Cell. Biol*. 2004, **6**, 1221-1228.

58 I. Tanida, T. Ueno and E. Kominami, *Methods Mol. Biol*., 2008, **445**, 77-88.

59 H. Chaachouay, P. Ohneseit, M. Toulany, R. Kehlbach, G. Multhoff and H.P. Rodemann, *Radiother Oncol*., 2011, **99**, 287-292.

Polyethylenimine mediated magnetic nanoparticles for combined intracellular imaging, siRNA delivery and anti-tumor therapy

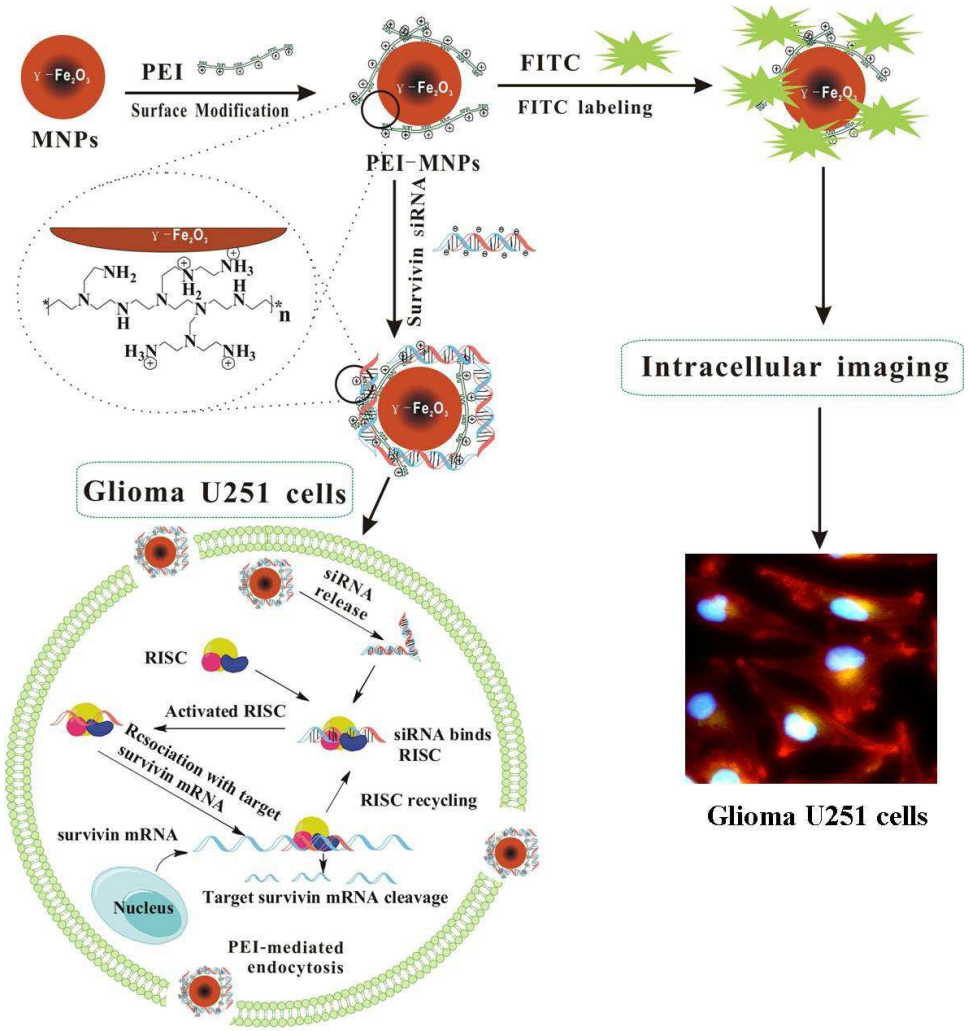

Figure 1 Schematic representation of the PEI-MNPs mediated intracellular imaging, and as carriers for survivin siRNA delivery in glioblastoma multiforme U251 cells.

The general principle of the PEI-MNPs mediated intracellular imaging, siRNA delivery and anti-tumor therapy for human malignant glioblastoma multiforme U251 cells (Figure 1) starts with the preparation of PEI-MNPs by combining magnetic γ-Fe_2O_3 nanoparticles (MNPs) and

PEI, and the composed PEI-MNPs were then modified with flourescent FITC. Subsequently, the FITC labeled PEI-MNPs (FITC-PEI-MNPs) were internalized into U251 cells for intracellular imaging. Simultaneously, the PEI-MNPs were also loaded with survivin siRNA through electrostatic attraction, which was finally delivered into the glioblastoma cells. The results showed that fluorescent FITC-PEI-MNPs could efficiently enter the tumor cells and approach the nuclei after being uptaken, and the fabricated siRNA~PEI-MNPs displayed a very much better therapeutic efficiency to inhibit cell proliferation, and induce cell apoptosis and autophagy of glioblastoma U251 cells. Therefore, this study suggested that the fabricated PEI-MNPs were a promising non-viral nanovehicle for the combined intracellular imaging and siRNA delivery for an efficient anti-tumor therapy based on siRNA therapeutic strategy.